Chromatographic parameter determination for complex biological feedstocks

Pirrung, Silvia M.; Parruca da Cruz, Diogo; Hanke, Alexander T.; Berends, Carmen; Van Beckhoven, Ruud F.W.C.; Eppink, Michel H.M.; Ottens, Marcel

DOI
10.1002/btpr.2642

Publication date
2018

Document Version
Final published version

Published in
Biotechnology Progress

Citation (APA)
Pirrung, S. M., Parruca da Cruz, D., Hanke, A. T., Berends, C., Van Beckhoven, R. F. W. C., Eppink, M. H. M., & Ottens, M. (2018). Chromatographic parameter determination for complex biological feedstocks. *Biotechnology Progress*, *34*(4), 1006-1018. https://doi.org/10.1002/btpr.2642

Chromatographic Parameter Determination for Complex Biological Feedstocks

Silvia M. Pirrung
Dept. of Biotechnology, Delft University of Technology, Van der Maasweg 9, Delft, 2629 HZ, the Netherlands

Diogo Parruca da Cruz
Dept. of Biotechnology, Delft University of Technology, Van der Maasweg 9, Delft, 2629 HZ, the Netherlands

Alexander T. Hanke
Dept. of Biotechnology, Delft University of Technology, Van der Maasweg 9, Delft, 2629 HZ, the Netherlands

Carmen Berends
Dept. of Biotechnology, Delft University of Technology, Van der Maasweg 9, Delft, 2629 HZ, the Netherlands

Ruud F.W.C. Van Beckhoven
DSM Biotechnology Center, Alexander Fleminglaan 1, AX Delft, 2613, the Netherlands

Michel H.M. Eppink
Synthon Biopharmaceuticals BV, Microweg 22, GN Nijmegen, 6503, the Netherlands

Marcel Ottens
Dept. of Biotechnology, Delft University of Technology, Van der Maasweg 9, Delft, 2629 HZ, the Netherlands

DOI 10.1002/btpr.2642
Published online 1 July 2018 in Wiley Online Library (wileyonlinelibrary.com)

The application of mechanistic models for chromatography requires accurate model parameters. Especially for complex feedstocks such as a clarified cell harvest, this can still be an obstacle limiting the use of mechanistic models. Another commonly encountered obstacle is a limited amount of sample material and time to determine all needed parameters. Therefore, this study aimed at implementing an approach on a robotic liquid handling system that starts directly with a complex feedstock containing a monoclonal antibody. The approach was tested by comparing independent experimental data sets with predictions generated by the mechanistic model using all parameters determined in this study. An excellent agreement between prediction and experimental data was found verifying the approach. Thus, it can be concluded that RoboColumns with a bed volume of 200 μL can well be used to determine isotherm parameters for predictions of larger scale columns. Overall, this approach offers a new way to determine crucial model input parameters for mechanistic modelling of chromatography for complex biological feedstocks. © 2018 The Authors Biotechnology Progress published by Wiley Periodicals, Inc. on behalf of American Institute of Chemical Engineers *Biotechnol. Prog.*, 34:1006–1018, 2018
Keywords: chromatography, high-throughput process development (HTPD), downstream processing (DSP), mechanistic modeling

Introduction

Detailed models to predict chromatographic behavior are available nowadays. However, accurate model input parameters are needed to simulate chromatograms with little uncertainties. Some of these, for instance packing and mass transfer parameters, can be easily determined.[1] Others such as adsorption parameters pose a bigger challenge especially for complex biological feedstocks.

A commonly applied approach to determine such adsorption parameters is the inverse method.[2–4] Using such an approach that minimizes the difference between experimental chromatograms and the mechanistic model can give erroneous parameters in case the experimental conditions are not determined accurately even if the found residual is small.[5] Additionally, impurities eluting at almost identical conditions can hardly be identified with distinctive parameters. Another approach is the determination via batch uptake experiments, which can be performed in a high-throughput format.[6,7] However, the obtained parameters might not be as reliable as the ones determined in chromatography columns, since sufficient mixing cannot be ascertained in case of very low-protein concentrations and/or large biomolecules.[7] In such cases, isocratic and linear gradient experiments on columns might be preferable.

Correspondence concerning this article should be addressed to M. Ottens at m.ottens@tudelft.nl

Previously, such approaches involving column experiments have even been applied to complex feedstocks by performing multiple fractionation steps.[8] Subsequently, in efforts to save precious sample, Hanke et al. developed a 3D liquid chromatography approach that consists of: a pH gradient prefractionation as a first dimension to reduce sample complexity; a second dimension with gradient experiments to obtain isotherm parameters on RoboColumns, which have a bed volume of only 200 μL, and a final dimension of size exclusion chromatography to increase the resolution.[9]

The aim of this article is to develop an improved high-throughput strategy for the determination of model input parameters for complex biological feedstocks. This article extends the approach by Hanke et al. to its use on robotic liquid handling systems to allow parallelization and time savings. The approach is also expanded to obtain parameters describing adsorption at the full range of protein concentrations, at which industrial processes are normally operated. For that, maximal binding capacities of the resin of interest are determined from fractions of the first dimension in batch-uptake experiments in a high-throughput format. To see if protein-protein interactions have a significant impact on the adsorption behavior, the second virial coefficient of the main product, a monoclonal antibody, is determined. The second virial coefficient is commonly used to describe protein aggregation behavior.[10,11] Moreover, it has once been used in the formulation of a chromatography isotherm.[12] In this study, it is introduced as an alternative to the protein interaction parameter in Mollerup's thermodynamic framework[13] by reformulating the isotherm. Finally, the chromatography model with the newly determined parameters from crude clarified cell harvest is compared to experimental chromatographic results to show the validity of the overall approach.

Mechanistic Chromatography Model

The equilibrium transport dispersive model can describe the behavior inside a chromatography column with the following mass balance for the mobile phase (Eq 1):

$$\frac{\partial \boldsymbol{c_i}}{\partial \boldsymbol{t}} + \frac{1-\varepsilon_\mathbf{b}}{\varepsilon_\mathbf{b}} \frac{\partial \boldsymbol{q_i}}{\partial \boldsymbol{t}} = -\boldsymbol{v} \frac{\partial \boldsymbol{c_i}}{\partial \boldsymbol{x}} + \boldsymbol{D}_{\mathrm{L},i} \frac{\partial^2 \boldsymbol{c_i}}{\partial \boldsymbol{x}^2} \tag{1}$$

where c_i is the concentration in the bulk phase of protein i, ε_b is the bed porosity, v is the interstitial velocity of the mobile phase and can be calculated as $v = u/\varepsilon_b$ with u, the superficial velocity. $D_{L,i}$ is the axial dispersion coefficient. The concentration distributions inside the particles are not being considered in this model. This model is typically chosen for its simplicity and often sufficiently high accuracy.[14]

The linear driving force approach for the mass transfer in the liquid phase was used to approximate the change in q_i, the concentration of protein i in the stationary phase, over time (Eq 2).

$$\frac{\partial q_i}{\partial t} = k_{\mathrm{ov},i}\left(c_i - c_{\mathrm{p},i}{}^*\right) \tag{2}$$

where $k_{ov,i}$ is the overall mass transfer coefficient. To calculate $c_{p,i}{}^*$, the concentration in the particle pores, an appropriate adsorption isotherm can be used. One example is the following mixed-mode isotherm developed within Mollerup's thermodynamic framework,[13] which is valid for mixed-mode chromatography, ion-exchange chromatography, and hydrophobic interaction in a nonlinear concentration range.[15]

$$\frac{q_{\mathrm{p},i}}{c_{\mathrm{p},i}} = A_i \left(1 - \sum_{j=1}^{m} \frac{q_{\mathrm{p},j}}{q_{\mathrm{p},j}^{\max}}\right)^{v_i + n_i} \tag{3}$$

The fraction of free ligands is shown in the term $1 - \sum_{j=1}^{m} \frac{q_{p,j}}{q_{p,j}^{max}}$, where q_p^{max} represents the maximum binding capacity; m stands for the number of proteins; and j for the protein species. n_i is the stoichiometric coefficient in hydrophobic interaction chromatography. v_i is the stoichiometric coefficient for ion exchange chromatography, which can be calculated as z_p/z_s with z_p, the effective binding charge of the protein, and z_s, the charge on the salt counter ion.

The initial slope of the isotherm or partition coefficient, A_i, can be calculated by:

$$A_i = K_{\mathrm{eq},i} \Lambda^{(v_i + n_i)} \left(z_s c_s\right)^{-v_i} c_v{}^{-n_i} \gamma_i \tag{4}$$

where K_{eq} is the thermodynamic equilibrium constant, Λ is the ligand density, c_s is the salt concentration, and c_v is the molarity of the solution in the pore volume. The activity coefficient can be calculated as $\gamma_i = e^{K_{s,i} c_s + K_{p,i} c_{p,i}}$ given K_s, the salt-protein interaction coefficient or salting-out constant, and K_p, the protein–protein interaction coefficient. If salts with small salting out effects such as chlorides are used, K_s becomes negligible.[16] At very low protein concentrations, the contributions of protein–protein interactions are expected to be minimal, which is why K_p can be considered negligible. At these conditions A_i can be simplified to:

$$A_i = K_{\mathrm{eq},i} \Lambda^{(v_i + n_i)} \left(z_s c_s\right)^{-v_i} c_v{}^{-n_i} \tag{5}$$

The retention of a protein is determined by its size exclusion as well as its thermodynamic properties as described by the partition coefficient. The retention factor can, thus, be related to the partition coefficient with the following equation[17]:

$$k_i = \frac{(1-\varepsilon_b)\varepsilon_p K_{D,i}}{\varepsilon_b}(1 + A_i) \tag{6}$$

where the distribution coefficient $K_{D,i}$ describes the accessibility of the resin for each protein i.

At higher protein concentrations, however, the influence of protein-protein interactions should be taken into account. In the case of complex mixtures where one protein species is predominant, it can be assumed that protein-protein interactions are solely of importance between proteins of this single protein species i. Then, the molar activity coefficient can be approximated by Refs. 18 and 19:

$$\ln \gamma_i = 2B_{ii} c_{\mathrm{p},i+\ldots} \tag{7}$$

where B_{ii}, or B_{22}, is the second osmotic virial coefficient, which takes into account deviations from ideal behavior that stem from interactions of two protein molecules of the same species.[20] It was assumed that interactions of more than two molecules are negligible. With that and due to the low salting-out effect of chloride, the activity coefficient for the predominant protein species was simply defined as:

$$\gamma_i = e^{2B_{22} c_{\mathrm{p},i}} \tag{8}$$

Material and Methods

Gradient chromatofocussing prefractionation

The complex sample used for this study is a clarified CHO cell culture supernatant containing a monoclonal

Table 1. Resin and Corresponding Buffer Specifications

Resin	Supplier	Type	dp [μm]	pH	Buffer type	Buffer [mM]	Salt type	Salt range [mM]
Poros 50HS	Applied Biosystems	Strong CEX	50[26]	4.5	Acetic acid	25	Sodium chloride	0 - 500
Capto MMC	GE Healthcare	MMC	85[25]	6.75	MOPS	25	Sodium chloride	0 - 350

immunoglobulin G (IgG1) with a concentration of 1.3 mg/mL. The pI of IgG1 was determined to be 8.6 by capillary isoelectric focusing. Prior to use, the samples were rebuffered using disposable PD-10 columns, following the manufacturers protocol (GE Healthcare, Sweden). As a first separation dimension, the samples were fractionated by linear pH-gradient chromatography on a Mono Q 4.6/100 strong anion exchange column (GE Healthcare, Sweden) or a Mono S 4.6/100 strong cation exchange column (GE Healthcare, Sweden). The prefractionation was performed as described by Hanke et al.[9,21]

High-throughput isocratic chromatography

Column Characterization. The columns used were 200 µL RoboColumns (Repligen, Germany), packed with two different resins as described in Table 1. The porosity and pore accessibility of these columns were analyzed on an Äkta Explorer 10 (GE Healthcare, Sweden) with a custom made adaptor. It was equipped with a 1100 series refractive index detector (Agilent, CA) to measure the retention volumes of dextrans with varying sizes (180–6,300,000 Da). The distribution coefficient K_D was calculated as in Ref. 22:

$$K_{\mathrm{D}}=\frac{\frac{\mu_1}{V_{\mathrm{col}}}-\varepsilon_{\mathrm{b}}}{1-\varepsilon_{\mathrm{b}}} \tag{9}$$

where μ_1 is the mean retention volume or first moment of the peak corrected for the system dead volume, which is usually determined with a tracer without having a column attached, and the dead volume in the column itself. The column dead volume is very important in miniature columns such as the RoboColumns, since the ratio of column volume (V_{col}) to column dead volume is smaller. In previous studies, it was found to be 30 μL.[9] The bed porosity ε_{b} generally lies in between 0.3 and 0.4 for packed chromatography columns.

The intraparticle porosities, $\varepsilon_{\mathrm{p},n}$, and pore radii, $r_{\mathrm{pore},n}$, were determined by fitting the following Eqs 10 and 11[23] to the K_{D} data using MATLAB's function *lsqcurvefit*:

$$K_{\mathrm{D},n}=\left(1-\frac{r_h}{r_{\mathrm{pore},n}}\right)^2 \tag{10}$$

The amount of different pore types, n, is two for a resin with bidisperse pores such as POROS 50 HS. The hydrodynamic radii r_h for the dextranes were calculated with their molecular mass M according to an empirical correlation reported in Ref. 24 ($r_h=0.0271\ M^{0.498}$). The total intraparticle porosity for a resin with two pore types was than calculated as $\varepsilon_p=\varepsilon_{p,1}+\varepsilon_{p,2}$ where $n=1$ represents the macropores and $n=2$ the micropores. The overall K_D for both pores is defined as[25]:

$$K_{\mathrm{D}}=\varepsilon_{\mathrm{p},1}K_{\mathrm{D},1}+\varepsilon_{\mathrm{p},2}K_{\mathrm{D},2} \tag{11}$$

Isocratic Chromatography. The high-throughput liquid chromatography experiments were performed on a Freedom Evo 200 liquid handling workstation equipped with an 8-channel liquid handling arm fitted with 1 mL syringes and Te-Chrom station (Tecan Switzerland). These systems are neither equipped with dual-piston pumps, nor with inline detectors. Instead single piston pumps apply a liquid flow, fractions are collected at the column outlet by a 96-well plate placed on a motorized shuttle, and analysis takes place offline. These mechanical simplifications require some adaptions to the experimental approach, to allow generation of data that is straightforward comparable to experiments performed on traditional systems.

Prior to each chromatographic experiment, a sufficient volume of buffer for both column equilibration and elution was mixed from stock solutions by the liquid handling system. The two stock solutions were prepared with MiliQ at a low salt and a high salt concentration. The mixing ratios were chosen to result in eight different final salt concentrations in the desired ranges. Specifications for each resin and the respective buffers are given in Table 1.

Samples collected from the prefractionation gradient were transferred into a low salt buffer through at least 3 buffer exchange cycles in Amicon spin filters with a nominal molecular weight cut-off of 3 kDa (Millipore) following the protocol recommended by the manufacturer. After rebuffering, each sample was split into eight aliquots and appropriate volumes of low and high salt buffer were added to result in eight samples of equal protein content and pH, but with salt concentrations corresponding to the eight prepared elution buffers.

Prior to injection each column was equilibrated with 5 column volumes (CV) of elution buffer. The injection volume to each column was 20 µL. The samples were eluted with a total of 15 CV of elution buffer at a flowrate of 0.15 mL/min per column. During the isocratic elution a total of 22 samples were collected from each column. The first twelve fractions had a target volume of 75 µL and were collected in a half area UV-star plate (Greiner-Bio One, the Netherlands). Afterwards six additional fractions with a target volume of 150 µL were collected in a full area UV-Star plate (Greiner Bio-One, the Netherlands), followed by four more with a target volume of 300 µL. This staggered fractionation strategy was chosen as a compromise between high resolution at the beginning of the experiment where sharp and narrow peaks were expected and a low total number of fractions. The columns were subsequently cleaned with 5 CV of washing buffer of which the first 600 µL were collected in two fractions with a target volume of 300 µL each. Once this step had been completed both fractionation plates were passed on to the plate reader for analysis. Prior to the next experiment each column was sanitized with 5 CV of sanitation buffer.

Fraction Volume Estimation. One of the main technical challenges in the operation of RoboColumns on a conventional liquid handling system, is that the fractionation intervals, the moments at which the collection plate shuttle moves from one column of wells to the next, are defined in relation to the syringe motor position that applies flow to the columns. As there is no reliable mechanism to synchronize the falling of drops from the column outlet, and the size of the drops themselves may vary with changes in buffer composition and protein content, the volume that actually ends up in each well may vary significantly, especially when the target fraction volume is small. It is therefore necessary to

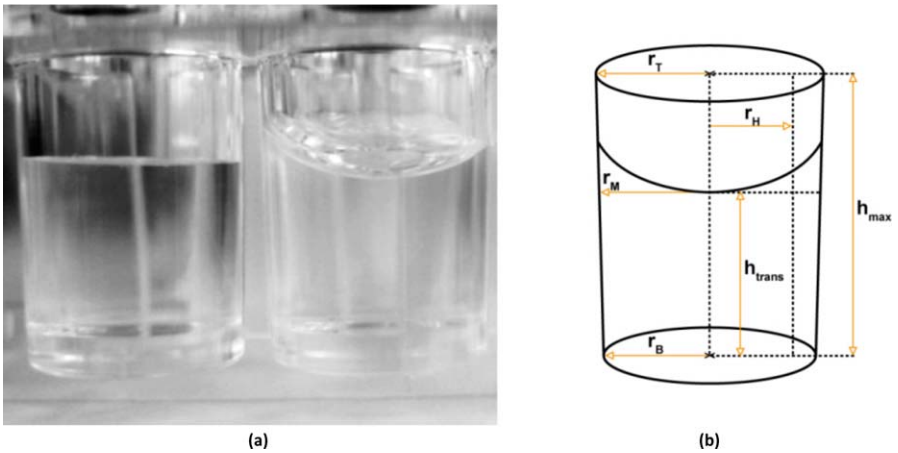

Figure 1. Impact of liquid distribution in a well on the transmission path in the geometric well center.

a: Two wells with equal liquid volume of buffer with no protein present (left) and 0.1 g/l of lysozyme (right); b: Schematic illustration of the geometry of a well showing the height and radius parameters used for the estimation of the liquid volume.

measure the volume of each well in order to reduce the experimental noise that would be caused by assuming a constant fraction volume.[27] So far this was either performed by detection of the liquid level by probing with the pipetting needles,[27] or by correlation of the transmission path with the near-infrared-red (NIR) adsorption of the buffer.[28,29] Both approaches have been demonstrated to be suitable for the normalization of absorption measurements towards the transmission path, but both lack the ability to detect and quantify the shape of the meniscus in each well, limiting their ability to accurately measure the total volume of liquid in a well. To overcome this limitation an extension of the NIR absorption based volume detection technique is introduced in this section.

All optical measurements in 96-well plates were performed in an infinite M200 plate reader (Tecan, Switzerland). The absorption values at 600 nm, 900 nm, and 997 nm wavelengths were measured at the geometric well center. The adsorption at 600 nm is measured at an additional 20 points, evenly distributed along a circle around the geometric well center using the built-in multiple reads per well function of the plate reader. The minimum distance of these measurement points from the well walls was set to 330 μm. These measurements are used in combination with knowledge of the well geometry as provided by the plate manufacture to estimate the volume of each well. An overview of the geometric parameters of the well that are used for these calculations is given in Figure 1b).

In accordance with the Lambert-Beer law a linear correlation between the transmission path (h_{trans}) and the corrected NIR absorption (ΔNIR) of the buffer is assumed, with a specific transmission coefficient ($\tau_{\mathrm{NIR,buffer}}$) related to the density of the buffer.

$$h_{\mathrm{trans}} = \tau_{\mathrm{NIR,buffer}} \cdot \Delta\mathrm{NIR} \tag{12}$$

The ΔNIR is the difference between the absorption at 997 nm and 900 nm. The walls of the used 96 well plates are slightly slanted. The radius of the wells cross section at the height of the bottom of the meniscus (r_{M}) is calculated from h_{trans} and the wells upper (r_{T}) and lower radius (r_{B}) by:

$$r_{\mathrm{M}} = (r_{\mathrm{T}} - r_{\mathrm{B}}) \frac{h_{\mathrm{trans}}}{h_{\mathrm{max}}} + r_{\mathrm{B}} \tag{13}$$

with h_{max} being the total height of the well.

For a perfectly flat meniscus, such as in the left well shown in Figure 1a the volume can now be estimated by the formula for the volume of a circular truncated cone. For wells with a more pronounced meniscus, such as the right one in Figure 1a, an extra term needs to be added. The 600 nm measurements are corrected for the value at the center of the well and summed up (Σ_{halo}). For a flat meniscus this value is close to zero. For more pronounced menisci the value exponentially increases, so a correction factor (C_{Vm}) based on its natural logarithm is introduced, leading to the following equation for the estimation of liquid volume (V_{est}) in a well:

$$V_{\mathrm{est}} = \frac{1}{3}\pi\left(r_{\mathrm{B}}^2 + r_{\mathrm{B}} r_{\mathrm{M}} + r_{\mathrm{M}}^2\right) h_{\mathrm{trans}} + C_{\mathrm{Vm}} \cdot \ln\left(\Sigma_{\mathrm{halo}}\right) \tag{14}$$

The method is calibrated with both a half and full area plate containing known volumes ranging from 0 μL to the maximum well capacity, of both protein free buffer and buffer with addition of a small concentration (~0.1 g/L) of model proteins, such as bovine serum albumin or lysozyme. The buffer NIR extinction coefficient $\tau_{\mathrm{NIR,buffer}}$ is assumed to be identical for half and full area plates, whereas the meniscus coefficient (C_{Vm}) is determined separately for each plate geometry. Both coefficients are determined by a least-square regression of Eqs (12–14) in MATLAB (Mathworks, USA). Afterwards the coefficients are validated against a second set of plates with a different distribution of sample volumes. The accuracy of each measurement was calculated by:

$$\mathrm{Acc}(V_{\mathrm{est}}) = \left(1 - \frac{V_{\mathrm{est}} - V_{\mathrm{nominal}}}{V_{\mathrm{nominal}}}\right) \times 100[\%] \tag{15}$$

Reconstruction of High-Throughput Chromatograms. As high-throughput chromatography systems, such as the TeChrom used in this study, do not possess in-line detection systems, chromatograms need to be reconstructed from the measurements performed on the collected fractions. The transmission path and total well volume of each collected fraction were calculated as according to the approach outlined in the preceding section. To reduce the noise in the absorption signals each value is corrected for the absorption at 330 nm and normalized against the estimated transmission path. To determine the position of each normalized absorption in the reconstructed chromatogram, the volume of all

preceding fractions is summed up and added to half the volume of the corresponding fraction.

Deconvolution and Peak Moment Calculations. To estimate the number of peaks in each chromatogram, each data set was scanned for data points fulfilling the following criteria: they had to have a normalized 230 nm absorption of at least 0.1 mAU/cm and this value needed to be larger than both the neighboring fractions. For practical purposes related to the small number of available data points per chromatogram only the largest four points fulfilling these criteria were considered for further analysis. The heights and positions of the local maxima identified by this algorithm were used as initial guesses for a least-squares based fitting of peak model to the reconstructed chromatogram. To estimate good parameters for components with much lower concentrations than the IgG1, parameter fitting was carried out several times for different ranges of the size exclusion chromatogram. This also reduced the time needed for the parameter fitting in general, since much less peaks were included each time.

The function chosen for fitting was based on a one-dimensional adaption of the model for multiple superimposed exponentially modified Gaussian peaks described in Ref. 21. Instead of minimizing the squares between the measured data point and the curve described by the peak model, the average of the model curve was calculated over each fraction interval, and the squares between this value and the measurement were minimized. The fitting was carried out in MATLAB using the built-in *lsqcurvefit* function. All parameters were normalized for the regression. Computation was performed in parallel on four cores using MATLAB's Parallel Computing Toolbox™. The areas and first moments of the fitted peaks were calculated together with their standard errors of regression following the same principles as in Ref. 21.

Parameter Fitting. The resulting peak moments were used to calculate the retention factors, k_i, defined by Ref. 22:

$$k_i = \frac{\mu_{1,i} - V_0}{V_0} \tag{16}$$

V_0 is the column void volume ($\varepsilon_b V_{col}$). With that, the combination of Eqs 5 and 6 allows the regression of relevant isotherm parameters based on the peak moments at the used experimental conditions. For the cation exchange resin POROS 50 HS, the stoichiometric coefficient for HIC, n, can be set to 0. At the investigated pH and salt type, chromatographic behavior seemed to be sufficiently well described on Capto MMC using only the ion exchange part of the adsorption isotherm, although Capto MMC is a mixed mode resin. Therefore, also here n was set to 0 simplifying the isotherm.

The regression was performed with MATLAB's *lsqcurvefit function*. The termination tolerance for the objective function value (*FunTol*) and the parameter (*TolX*) were set to 10^{-12} and the maximum number of iterations allowed to 1000.

Batch uptake experiments

Additionally, the fractions containing the IgG1 were analyzed further to determine the maximal capacity. For that, batch uptake experiments were performed in 96 well filter plates. The resin volume of 7.8 μL was dispensed with help of the MediaScout Resiquot (Repligen, Germany) as described in Ref. 30. Even though the volume dispensed by the Resiquot is quite accurate, less particles might be present than in a packed column because of a smaller packing density.[31,32] In this study, a factor of 1.06 was applied as suggested by the supplier for POROS 50 HS.[33] For Capto MMC, no packing factor was used.

For each resin, the residual amount of liquid staying inside the resin after centrifugation, the liquid hold-up volume, was determined according to a protocol described by Nfor et al.[15] Before usage, the resin plaques were equilibrated with 300 μL of the respective buffer. For that, they were incubated at 1300 rpm for 5 min and afterwards centrifuged at 4000g. The equilibration procedure was repeated once. The corresponding buffer solutions are shown in Table 1. The salt concentration for Capto MMC and Poros 50 HS was 0 M. The plates were incubated for two hours at 1300 rpm at room temperature. To minimize evaporation, they were covered with a self-adhesive foil. In order to verify the maximal capacities, additional batch uptake experiments were performed with a sample of the product that was purified with a protein A column.

The regression was performed with MATLAB's *nlinfit function*, because it allows weighted regression. Weights were proportional to the standard error attached to each data point. Otherwise, the same settings as in Parameter Fitting section were applied. The fitting function here was Eq 3 with only q_p^{max} as variable.

Self-interaction chromatography

In the clarified cell harvest, IgG1 has a much greater concentration than any other protein. Therefore, it was assumed that only the activity coefficient for IgG1 needs to be known and thus, its second osmotic virial coefficient B_{22}. The B_{22} was determined by self-interaction chromatography using prepacked HiTrap NHS-activated HP columns (GE Healthcare, Sweden) on an Äkta Avant 25 chromatography system (GE Healthcare, Sweden). The HiTrap columns were flushed with 6 mL of an ice-cold 1 mM HCl solution to wash out the storage solution, isopropanol, as suggested by the manufacturer. A buffer of 0.2 M NaHCO3 and 0.5 M NaCl at pH 8.5 was used as a coupling buffer. The IgG1 sample, which was purified with a Protein A column, was supplied by Synthon. The coupling buffer was exchanged with Amicon Ultra-4 Centrifugal filters (Merck Millipore, the Netherlands) by centrifuging multiple times for 15 min at 4000g. Each time, the sample was diluted 2:1 with the coupling buffer to prevent aggregation. The final solution contained 3 g/L IgG1. For coupling, it was recirculated with a flowrate of 1 mL/min over the column for 4 h at around 4°C to ensure uniform coupling.[34] The coupling solution was washed out with 3 CV of coupling buffer. The concentration of the eluent containing the IgG1 was measured at UV 280 nm to determine the amount of IgG1 that was immobilized onto the column. Subsequently, the surface coverage was calculated as described by Ref. 11 to be 12.3%, which falls in the range of recommended surface coverage.[34] Finally, any excess active groups were deactivated according to the protocol by the manufacturer of the columns.

According to the approach described by Ahamed et al.,[11] the retention volume of the IgG1 without protein-protein interactions was measured in an additional HiTrap column without immobilized antibody. It was generated according to the same deactivation protocol. This column assumedly acts only as a size exclusion column. For each solution condition, experiments were performed in the blocked column and

Table 2. Mass Transfer Correlations

Parameter	Correlations
Free Diffusivity	Young[36]
Film Mass Transfer Coefficient	Wilson & Geankoplis[37]
Pore Tortuosity	Suzuki & Smith[38]
Pore Diffusivity	Brenner & Gaydos[39]
Axial Dispersion Coefficient	Gunn[40]
Hydrodynamic radius	Stokes Einstein[41]

adjusted with the following correlation to account for integrity differences:

$$V_0 = aV_{0,b} + b \tag{17}$$

where a and b are determined from the retention data of acetone and dextrane in the immobilized column as a function of their retention in the blocked column ($V_{0,b}$). For that, 50 μL of a 1% acetone solution and a solution of 2 g/L blue dextran in a 50 mM Tris-HCL and 100 mM KCl buffer at pH 7.5 were injected and eluted at 1 mL/min; in case of blue dextran, 1 M NaCl was added for the elution. Here, a was found to be 0.25 and b as 0.32.

The retention volumes were measured for IgG1 in both buffers (25 mM of MOPS or acetate buffer) with salt concentrations ranging from 0 to 1 M and from pH 4.5 to 7.5 on each column in duplicate. For that, the columns were first equilibrated with 10 CV of the respective buffer with a flowrate of 0.5 mL/min. The protein in the correct buffer with a concentration of 1.5 g/L was then injected and flushed with 5 CV of the respective buffer. Afterwards, the column was washed with 3 CV of 0.5 M NaCl.

A second-order polynomial function was fitted to the determined B_{22} values using MATLAB's *fit* function with the robust bisquare weights method. The polynomial was defined as following:

$$B_{22} = b_1 + b_2\ pH + b_3\ c_s + b_4\ pH\ c_s + b_5\ pH^2 + b_6\ c_s^2 \tag{18}$$

The resulting B_{22} was in the units (mol mL)/g^2. To use the determined B_{22} in the mechanistic model as shown in Eq 8, the units needed to be changed to L/mol by multiplying with the squared molecular weight and dividing by 1000.

Validation experiments

Validation experiments were performed on OPUS® ValiChrom 11.3/100 columns prepacked with the respective resins by Repligen (Germany) on an Äkta Avant 25 (GE Healthcare, Sweden). The flowrate was 400 cm/h. An additional validation run was performed with a column with a bed volume of 14.8 mL packed with POROS 50HS. The flowrate was 400 cm/h. Linear gradients of 12 CV were used during the elution in all validation experiments. All columns were stored in 20% Ethanol. Absorption was recorded at 210, 230 and 280 nm.

Protein quantification by size exclusion chromatography

All protein concentrations were determined in a UHPLC$^+$ (Thermo Fisher Scientific, MA, USA) system as described by Hanke et al.[9]

Modelling techniques

Mechanistic modelling was applied as described in Ref. 35. All correlations to determine relevant parameters are shown in Table 2.

Results and Discussion

Prefractionation and reference chromatogram

The prefractionation experiments and the corresponding two-dimensional reference maps are shown in Figure 2. For the anion exchange prefractionation (Figure 2a and b), Peak 2 corresponds to the IgG1, the protein of interest. The most abundant contaminants, Peaks 1, 3, 4, 6, and 7, appear to have very similar charge properties, as does at least one high molecular weight (HMW) contaminant, marked as Peak 5. The large difference in elution-pH of peaks 9–17 in relation to the protein of interest, indicates that these contaminants could easily be removed and, thus, they will be considered as noncritical impurities further on. Consequently, only the fractions of interest as marked in the prefractionation chromatogram (Figure 2a) were analyzed in detail. In the cation exchange prefractionation (Figure 2c and d), IgG1 is represented by ID 1. Here, much fewer contaminants were found to elute in the gradient indicating it to be a better mode of separation than anion exchange. Only one critical impurity, Peak 2, was identified. Therefore, only the two fractions as shown in Figure 2c were analyzed further.

High-throughput isocratic experiments

Well Volume Measurement. The regressed transmission coefficients for the used buffer system ($\tau_{NIR,buffer}$) was determined to be 0.640 ± 0.001 mm/AU. As the absorption in this wavelength is dominated by the water content of the buffer, it is practically the same for all aqueous buffer systems, provided that their density is still close to pure water. The meniscus correction coefficients (C_{Vm}) were determined to be 1.76 ± 0.30 µL/ln(Σ_{halo}) for the half area plates and 12.72 ± 0.35 µL/ln(Σ_{halo}) for the full area plates. The choice of model protein used to induce the formation of the meniscus was not found to have a significant effect on these parameters. Figure 3a shows the relation between the volume that is not accounted for by the truncated cone volume and therefore attributed to the meniscus, and the logarithm of the sum of the measurement around the well. The highly linear relationship for both well geometries supports the choice for a simple linear model. While the meniscus volume in the half area plates is in the range of 0–5 µL, it can account for up to 35 µL in the full-area plates, at least 10% of the total well volume. With the meniscus correction in place the accuracy of the volume detection is improved to better than 3% for the full-area plates and 5% for the half-area plates. Figure 3b and c shows the technique's accuracy over a range of different volumes in both plate geometries. While the accuracy appears to be largely volume independent in the half-area plates, there is clearly a negative effect caused by low volumes in full-area plates. This is caused by the tendency of small volumes to not evenly distribute across the well in full-area plates. As a result, it is recommended to use half-area plates for collection of fraction volumes in the range of 50 to 125 µL and full-area plates for volumes exceeding 125 µL.

Resin and Column Characteristics. The RoboColumns were characterized by pulse injections of dextran standards. The distribution coefficients, K_D, as calculated by Eq 9 are shown in Figure 4. The observed trend is typical for particles with bidisperse pores: First, K_D decreases with increasing hydrodynamic radius, which means that the bigger the particles the less access to the micropores they have; after

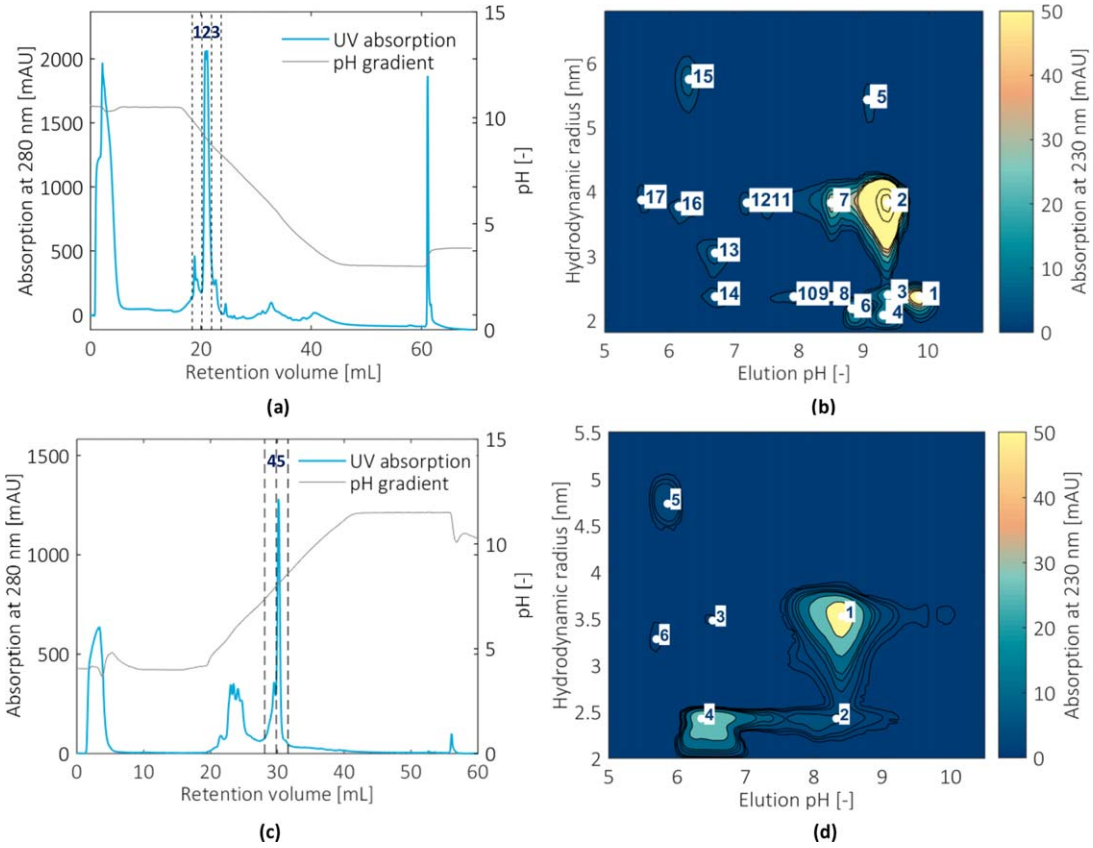

Figure 2. Prefractionation step on the AEX (a) and CEX (c) column.

Fractions of interest are marked by 1, 2, 3 and 4, 5 respectively; b and d: Two-dimensional reference chromatogram generated by an additional SEC analysis of the fractions from (a) and (c) respectively. Proteins are marked at their peak maximum according to the peak finding algorithm. The ones with the IDs 1–8 (c) and 1–2 (d) are contained in the fractions of interest. The absorption scale was cut at 50 mAU to also show contaminants at low concentrations. (d) Adapted from Ref. 21, with permission from Elsevier.

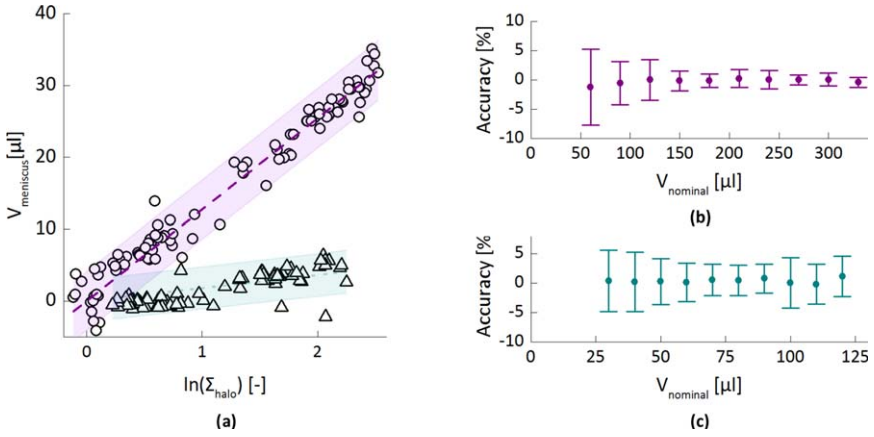

Figure 3. Calibration of the meniscus-sensitive volume detection method.

a: Linear correlation between the volume hidden by the meniscus and the natural logarithm of the sum of the absorption values on the measurement halo together with the 95% prediction bands for both full-area plates (dashed purple line and circles) and half-area plates (dotted teal line and triangles); **b and c**: Average volume estimation accuracy of method in full-area plates (b) and half-area plates (c). The error bars correspond to twice the standard deviation across at least 8 measurements.

around 10 nm, the curve starts levelling off, since now the access to the macropores is determining the behavior of the curve. Due to the big macropores, not even the largest dextrans are fully excluded from the particle pore volume. This is why the bed porosity cannot be calculated from the retention volume of the biggest dextran. For the RoboColumns, the bed porosity was assumed to be identical for all RoboColumns with the same resin (0.3 for POROS 50 HS and 0.35 for Capto MMC). For the validation columns, the bed porosity was determined to be 0.34 for POROS 50 HS and 0.36 for Capto MMC solving the Blake-Kozeny equation, which describes the change in pressure drop with linear flow.

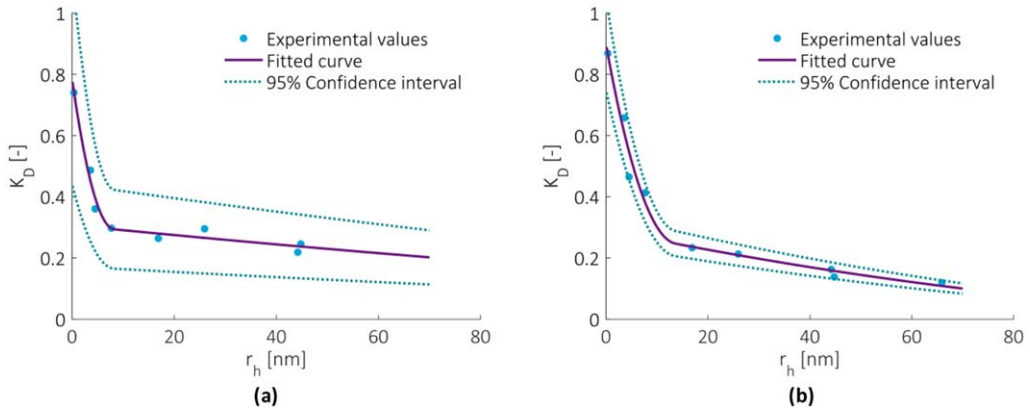

Figure 4. Calculated K_D values of the Dextran standards, the fitted K_D curve and its 95% confidence interval for POROS 50 HS (a) and Capto MMC (b).

Table 3. Resin Characteristics in POROS 50 HS and Capto MMC; Values are Given With Their Standard Error

	POROS 50 HS[42]	POROS 50 HS, this study	Capto MMC, this study
Macropore radius [nm]	470 ± 10.0	370.5 ± 78.00	168.8 ± 21.60
Macropore porosity [-]	0.32 ± 0.01	0.31 ± 0.01	0.29 ± 0.02
Micropore radius [nm]	11 ± 4.00	8.2 ± 0.40	13.6 ± 0.80
Micropore porosity [-]	0.41 ± 0.01	0.48 ± 0.02	0.61 ± 0.03
Total intraparticle porosity [-]	0.60 ± 0.01	0.79 ± 0.02	0.90 ± 0.03

Fitting Eqs 10 and 11 to the data resulted in the pore radii and porosities with their 95% confidence interval as presented in Table 3. The smaller pores (8.2 nm) are hardly accessible for IgG1 with its calculated hydrodynamic radius of 4.3 nm. The parameters as determined here mostly lie within the standard error of the parameters determined in Ref. 42 for POROS 50 HS although the porosity of the micropores is slightly higher, which might be explained by batch to batch variation. The total particle porosity varies more drastically, because it was calculated with a different equation than in Ref. 42. Overall, this shows that RoboColumns can well be used to determine resin properties such as porosities and pore sizes despite their small bed volume.

The same procedure was applied to RoboColumns filled with Capto MMC. In Ref. 25, it was assumed that the pore distribution in this resin is monodisperse and a good fit with the data was shown. However, only dextrans with a hydrodynamic radius of up to around 8 nm were used. Our data, which is very similar for smaller hydrodynamic radii, clearly shows with higher hydrodynamic radii that also Capto MMC has a bidisperse pore distribution. The behavior is very similar to POROS 50 HS, although the micropores have a slightly bigger radius and a higher porosity. Additionally, the macropores are smaller.

During the modelling, the pore diffusion was simply calculated as a combination of the diffusion in the macro- and the micropores taking into account their respective porosities:

$$D_p = \varepsilon_{p,1} D_{p,1} + \varepsilon_{p,2} D_{p,2} \tag{18}$$

The pore diffusion in the macro- and micropores was calculated as suggested in Ref. 22. Based on the findings in Ref. 42, intraparticle convection is assumed to be negligible at the comparably low flow rates applied in this study regardless of the big pore radius of the macropores.

The ligand density Λ is another critical parameter that defines the adsorption of the compounds to the resin and is thus needed for the calculation of the isotherm (Eqs 4 and 5). Data for it is available in literature: For POROS 50 HS, the ligand density per adsorber skeleton was reported to be 0.276 M with acid–base titration[31]; for Capto MMC, the ligand density per particle volume was reported as 0.128 M.[25]

Isocratic Chromatography. Each fraction of interest was analyzed with isocratic experiments at different salt concentrations on RoboColumns containing the respective resin (1, 2 and 3 on POROS 50HS; 4 and 5 on Capto MMC). Fractions collected here were further analyzed with size exclusion measurements, to increase resolution and sensitivity,[9] and UV measurements, to determine the well volume. Typical results of these experiments are shown in Figure 5. In the shown example, fraction 2 as marked in Figure 2a was subjected to different salt concentrations. With increasing salt concentration, the proteins (ID 3 and ID 4 detected in the shown range of hydrodynamic radii) elute earlier, which is typically expected in ion exchange chromatography. The additional UHPLC measurements resulting in the y axis make a clear distinction between the two proteins possible. Moreover, they allow the sequential regression of isotherm parameters for different ranges of hydrodynamic radii, which greatly improves the quality of parameters regressed for low concentrated proteins.

Figure 6 summarizes the results for all proteins of interest by plotting their first moments depending on the salt concentration. For Capto MMC, both proteins were present in fraction 4 and 5. Different retention volumes were found especially for the IgG1 (here shown with ID 1) depending on the fraction it was contained in. Since the protein concentrations were low in all RoboColumn experiments, this is most likely not due to competition or interaction effects between the proteins. Thus, it is unclear what causes this difference in behavior.

These first moments were then used to fit the relevant isotherm parameters K_{eq} and ν as reported in Table 4. For

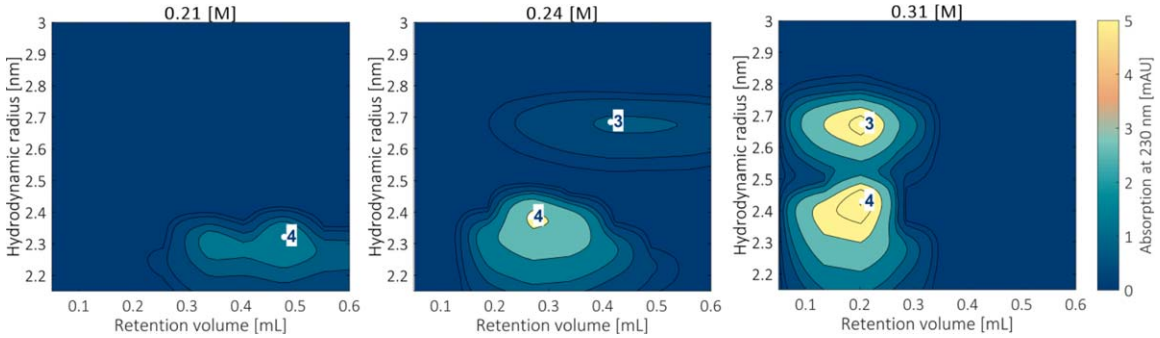

Figure 5. Example of 2D graphs generated in isocratic experiments (x axis) and subsequent UHPLC measurements (y axis) on POROS 50 HS.

The analyzed fraction was fraction 2 in Figure 2 containing the proteins with ID 2–5. For higher clarity only a portion of the 2D graph is shown.

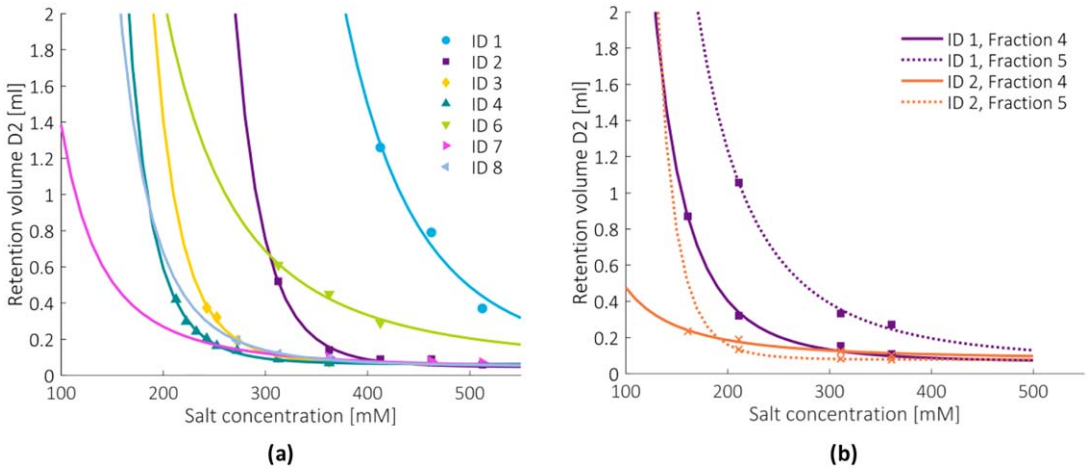

Figure 6. Experimental retention volumes (marker) and the respective fitted curves (lines) for all critical proteins on POROS 50HS (a) and Capto MMC (b).

Table 4. Isotherm Parameters Regressed from Retention Volume Curves Determined in RoboColumns With Their Standard Deviation

Resin	Protein	rh [nm]	K_{eq} [-]	ν [-]
POROS 50 HS	ID 1	2.4	12.6 ± 0.54	2.9 ± 0.5
POROS 50 HS	ID 2	4.2	34.6 ± 1.7	9.8 ± 1.3
POROS 50 HS	ID 3	2.7	2.2 ± 0.2	7.4 ± 0.7
POROS 50 HS	ID 4	2.2	177.1 ± 16.1	5.4 ± 1.1
POROS 50 HS	ID 6	2.2	0.9 ± 0.8	7.0 ± 0.3
POROS 50 HS	ID 7	4.2	2.0 ± 0.2	2.5 ± 0.2
POROS 50 HS	ID 8	2.4	0.2 ± 0.1	16.9 ± 6.4
Capto MMC	ID 1	4.2	51.5 ± 2.1	3.6 ± 0.4
Capto MMC	ID 2	2.8	16.6 ± 5.8	4.7 ± 1.6

rh: hydrodynamic radius; K_{eq}: equilibrium constant; ν: stoichiometric coefficient.

Capto MMC, the final parameters are the average of the parameters fitted for each fraction. The curves shown in Figure 6 were created with the fitted parameters. The protein with ID 5 could not be eluted under the salt concentrations applied during the experiments. Thus, no isotherm parameters could be fitted.

Batch-uptake experiments

Isotherms were determined under maximum binding conditions for both, an antibody purified with a Protein A step and the fractions from the prefractionation that contain mostly the antibody. Both sample types were chosen to understand if the small amounts of impurities present would influence the maximum binding capacity. For the modelling shown in Model Validation section, the maximum capacities were used that were determined with the fractions from the prefractionation as sample type. For all impurities, the resin capacity was assumed to be non-limiting, since their smaller size allows them access to pore space not available for IgG1.[43] Therefore, the maximal capacity of the resin was only analyzed for IgG1; results are shown in Figure 7 for both resins.

On POROS 50 HS, a maximum capacity of 49.0 ± 0.7 g/L was found for the purified mAb, while a maximum capacity of 44.2 ± 0.2 g/L was determined for the antibody contained in the fractions. This might be due to competition in the fractions between other impurities and IgG1. In literature, a slightly higher value of 58 g/L is reported for a different IgG.[26] One possible reason could be that the packing factor might be higher than 1.06 as stated by the supplier[33] when applying the resin with the ResiQuot, as was already observed previously.[31] Moreover, it could likely be caused by a difference in the antibody itself, the ionic strength of the solution or resin lot variability.

On Capto MMC, a maximum capacity of 66.4 ± 3.1 g/L was regressed for purified IgG1 and 77.4 ± 2.1 g/L for IgG1 in the fractions. The determined capacities fall into similar ranges as reported for another IgG in the literature on Capto MMC.[44] The disparities between both values might be

explained by the poor fit of the experimental values for the purified antibody with the predicted slope determined in the RoboColumn experiments. If a smaller slope was used during parameter regression, a higher maximal capacity would have been regressed. Still, the predicted slopes fit well with all other experimental data sets. A slight change of ionic strength in the buffer solution might be an explanation for the experiments with purified antibody on Capto MMC, since it was not measured in this study. Thus, it would be recommended to measure the ionic strength in each well directly in future studies.

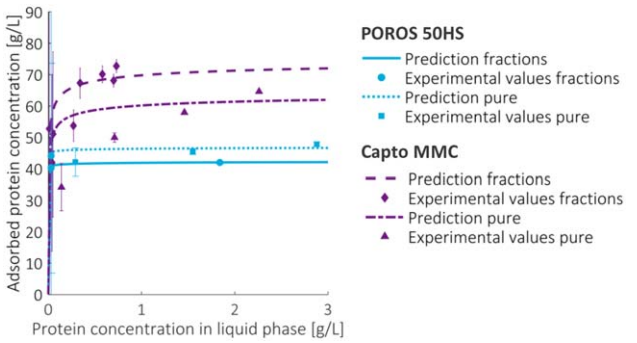

Figure 7. Determination of the maximal capacity for mAb on POROS 50 HS and Capto MMC.

The predicted lines were created by using the isotherm slope determined in the RoboColumn experiments with the maximum capacity as a fitting parameter. Values determined above 3 g/L are not shown.

Protein–protein interactions

Figure 8 summarizes the B_{22} values that were determined for IgG1 with varying salt concentrations and pH. On the left hand side, the resulting second-order polynomial functions were plotted for each buffer in the investigated range. The constants for both polynomials can be found in Table 5. In the acetate buffer (a), all B_{22} values fall into the so-called 'crystallization slot', which covers B_{22} values between -1×10^{-4} and -8×10^{-4} mol*mL/g^2 and is characterized by weak attractive protein interactions.[45] Also in the MOPS buffer (b), the B_{22} values are always negative indicating attraction. Here, however, the attraction is even weaker than in the acetate buffer suggesting higher protein stability. This difference might be explained by the zwitterionic nature of MOPS, since zwitterions do not contribute to the ionic strength of a solution.[46] Additionally, pH and salt

Table 5. All Constants for the Second-Order Polynomial as Defined in Equation 18

	b_1	b_2	b_3	b_4	b_5	b_6
Acetate buffer	6.791	−2.794	1.249	−0.575	0.237	1.474
MOPS buffer	2.119	−0.807	−0.199	0.222	0.046	−1.013

They need to be multiplied with 10^{-4}

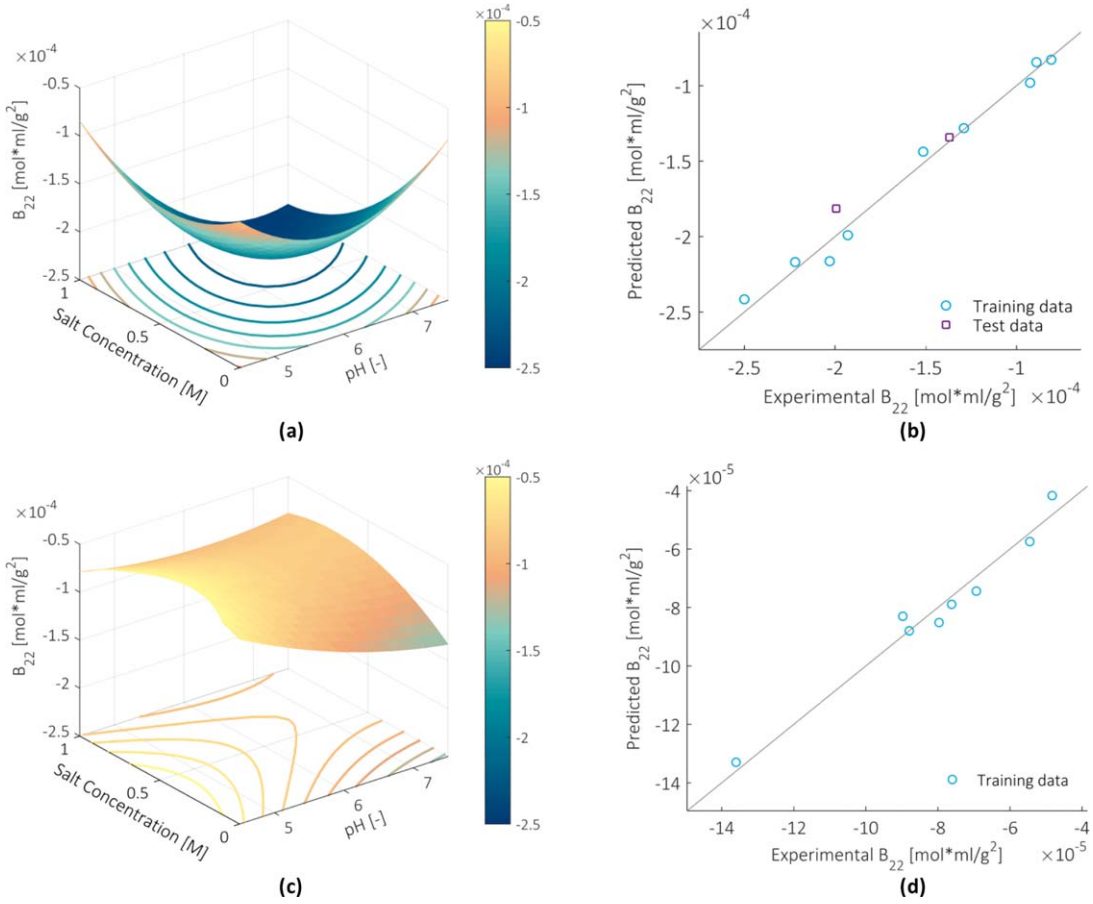

Figure 8. B_{22} values of IgG1 as a function of salt concentration and pH.

a and c: Second-order polynomial functions that were fitted on experimental data determined with the acetate buffer (a) and the MOPS buffer (c); **b and d**: Comparison of experimentally obtained B_{22} values with values given by the polynomial function for the acetate buffer (b) and the MOPS buffer (d).

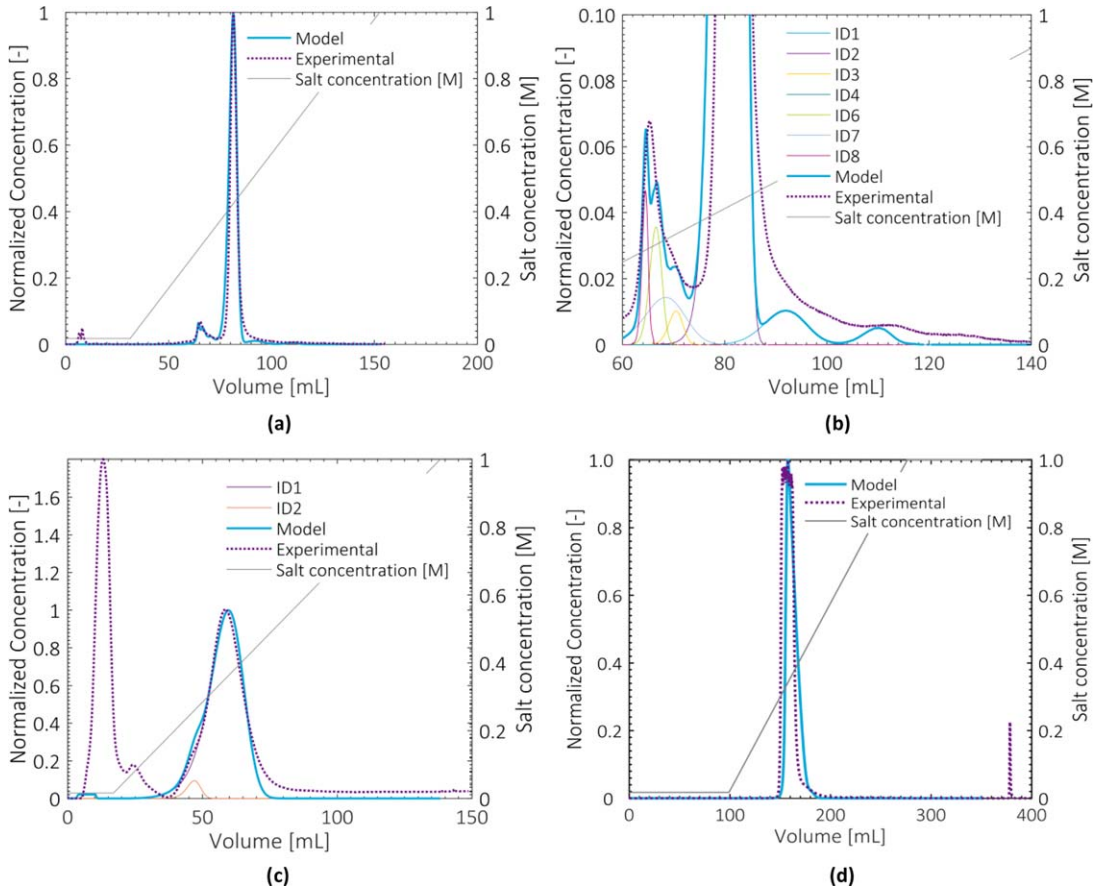

Figure 9. Model prediction versus experimental data.

a, b, and c: At low loading conditions on POROS 50HS for the complete chromatogram (a) and a zoom-in (b) as well as on Capto MMC (c); **d**: Load of 20 g/L of POROS 50HS on a 14.8 mL lab scale column

The critical proteins were simulated (POROS 50HS: ID 1–8; Capto MMC: ID 1–2). The buffer of the clarified cell harvest was exchanged before sample application.

concentration seem to have an almost negligible influence on the B_{22} values obtained in the MOPS buffer. Such comparably small changes for B_{22} values of monoclonal antibodies were already reported previously and explained with the ionic strength of the buffer system.[47] In that explanation, buffer and salt ions are shielding protein charges and, therefore, limit electrostatic interactions as well as the resulting changes in the B_{22} values. This theory might be true, since the change of pH has its strongest influence at the lowest salt concentration. Nevertheless, the influence of salt concentration and pH on B_{22} values is stronger in the acetate buffer, which has a higher ionic strength. Compared to literature data, however, where B_{22} data was shown to vary for instance between 10×10^{-4} and -15×10^{-4} mol*mL/g^2 for lysozyme with changing pH and NaCl concentration,[48] even the values reported here for the acetate buffer vary only slightly (1.5×10^{-4} mol*mL/g^2). A minimum of B_{22} values can be found at the highest salt concentration and the highest pH. This is logical, since salting out is typically strongest at the highest salt concentration. Additionally, the charge of IgG1 is lower the closer the pH is to its pI (for IgG1, the pI is typically between 8 and 9). The higher positive charge at lower pH values will result in increased repulsive interactions and, thus, an increased B_{22}.

On the right-hand side of Figure 8, experimental values are compared with the values predicted by the fitted second-order polynomial function. In general, a good correlation was found between predicted and experimental data. Since there was a higher variation in the B_{22} values of the acetate buffer, two additional experimental data points were determined that were not included in the data set used to fit the polynomial. As can be seen in Figure 8b, these two test data points were as well predicted by the polynomial as the data points used for the fitting.

Model validation

Finally, all determined parameters were used as model input parameters for the mechanistic model to simulate the critical proteins. Experiments were performed at identical conditions at lab scale with the clarified cell harvest to evaluate the accuracy of the model predictions.

In Figure 9a, b, and c, results can be seen for POROS 50 HS and Capto MMC under low loading conditions. The applied sample is the clarified cell harvest after a buffer exchange. In both predictions, tailing of IgG1 is underestimated, which becomes especially obvious in the zoomed chromatogram shown in Figure 9b. UHPLC analysis showed that this tailing was caused by dimerization or higher levels of aggregation. Besides that, an overall good agreement between predictions and experimental data can be observed. This can lead us to two conclusions. First, the critical

impurities were defined well in the prefractionation. If these critical impurities were to be removed by the respective chromatographic step, the purification step would be successful. Second, isotherm parameters for low-protein concentrations can be determined in RoboColumns without any extra modifications during scale-up. This was expected, because isotherm parameters cover the thermodynamics of protein adsorption in resin beads, which should be identical at an increased scale. Packing parameters and flow behavior are of course changed.

Additionally, the model was tested at different high protein loadings. The sample was purified with a Protein A column prior to sample application. One example is shown for a protein load of 20 g/L of resin on POROS 50HS in Figure 9. The predicted peak elutes slightly later than the experimental one. This can be caused by a small difference in void volume or ligand density, which can vary for example due to resin lot variation.[49] Another possibility could be that protein-protein interactions are not only taking place between two molecules, but even more. In that case, higher virial coefficients would need to be determined as well. The tailing of the peak was expected to be caused by a dimer or higher level of aggregates of the monoclonal antibody as in the experiment with low loading conditions. There was no isotherm data available for the dimer itself, since it did not form under the conditions applied in our parameter determination approach. Therefore, retention data of IgG1 was fitted again but with a K_D based on the doubled molecular weight (K_{eq}: 50.7 ± 2.6; υ: 8.3 ± 1.4). The simulations show that this seems to be a reasonable approximation.

Conclusion

This article presented an extensive approach to determine isotherm parameters for a clarified cell harvest containing a monoclonal antibody with a high-throughput workstation. First, the clarified cell harvest was prefractionated to simplify the mixture and define critical proteins. Second, the obtained fractions were analyzed with isocratic column experiments on RoboColumns, which led to isotherm parameters in the linear protein concentration range of the isotherm. Third, the maximal capacity of the resin was determined in batch uptake experiments. Fourth, the second osmotic virial coefficient was measured for IgG1 with self-interaction chromatography to describe protein-protein interactions. As a last step, the mechanistic model was tested at lab scale using all parameters obtained in this study. Results showed a high agreement between modelled and predicted chromatograms. Thus, the most obvious finding to emerge from this study is that RoboColumn data can indeed be used to model larger scale columns. Additionally, it verifies our assumption that it is sufficient to only focus on critical compounds.

Nevertheless, certain assumptions are only valid for a mixture like the one studied, where one protein, like the IgG1 in this study, is present in a much higher concentration than the others. If this was not the case, maximum capacities would need to be determined for other proteins as well. In that case, however, this would not be a problem, since these proteins would occur in higher quantities. Additionally, the assumptions made regarding the second virial coefficient would not be valid. Here, the B_{22} of a mixture would need to be calculated as for instance explained in Ref. 20.

An improvement that could be made to the current study is to move all experiments (excluding the prefractionation) on a high-throughput workstation to drive automation even further and decrease sample usage. For that, only self-interaction chromatography and size-exclusion chromatography would need to be adapted or exchanged, which would need further research.

Overall, the presented approach delivers reliable parameters for mechanistic modelling of chromatography. With that, it can aid the model-based development of processes, which promises reduced costs and time until a product can reach the market.

Acknowledgment

The authors acknowledge Synthon Biopharmaceuticals BV for the cell culture supernatant and the purified IgG1 solution. The authors gratefully thank Renske Rinzema and Xiaonan Li for testing our mechanistic model with many experimental data sets. A special acknowledgement goes to Carme Pons Royo, who performed the batch uptake and self-interaction experiments. We are also thankful for the laboratory help provided by Song Yi. This work was financially supported under grant F2.003 by the Ministry of Economic Affairs of the Netherlands and BE-Basic partner organizations (www.be-basic.org) through BE-Basic, a public private NWO-ACTS program.

Literature Cited

1. Osberghaus A, Hepbildikler S, Nath S, Haindl M, von Lieres E, Hubbuch J. Determination of parameters for the steric mass action model–a comparison between two approaches. *J Chromatogr A*. 2012;1233:54–65.
2. Kumar V, Leweke S, von Lieres E, Rathore AS. Mechanistic modeling of ion-exchange process chromatography of charge variants of monoclonal antibody products. *J Chromatogr A*. 2015;1426:140–153.
3. Osberghaus A, Hepbildikler S, Nath S, Haindl M, von Lieres E, Hubbuch J. Determination of parameters for the steric mass action model—A comparison between two approaches. *J Chromatogr A*. 2012;1233:54–65.
4. Marchetti N, Cavazzini A, Pasti L, Dondi F. Determination of adsorption isotherms by means of HPLC: adsorption mechanism elucidation and separation optimization. *J Sep Sci*. 2009;32:NA–741.
5. Borg N, Westerberg K, Andersson N, von Lieres E, Nilsson B. Effects of uncertainties in experimental conditions on the estimation of adsorption model parameters in preparative chromatography. *Comput Chem Eng*. 2013;55:148–157.
6. Lacki KM, Brekkan E. High throughput screening techniques in protein purification. *Methods Biochem Anal*. 2011;54:489–506.
7. Bergander T, Nilsson-Valimaa K, Oberg K, Lacki KM. High-throughput process development: determination of dynamic binding capacity using microtiter filter plates filled with chromatography resin. *Biotechnol Prog*. 2008;24:632–639.
8. Nfor BK, Ahamed T, Pinkse MWH, van der Wielen LAM, Verhaert PDEM, van Dedem GWK, Eppink MHM, van de Sandt EJAX, Ottens M. Multi-dimensional fractionation and characterization of crude protein mixtures: toward establishment of a database of protein purification process development parameters. *Biotechnol Bioeng*. 2012;109:3070–3083.
9. Hanke AT, Tsintavi E, Ramirez Vazquez M. d P, van der Wielen LAM, Verhaert PDEM, Eppink MHM, van de Sandt EJAX, Ottens M. 3D-liquid chromatography as a complex mixture characterization tool for knowledge-based downstream process development. *Biotechnol Prog*. 2016;32:1283–1291.

10. Quigley A, Williams DR. The second virial coefficient as a predictor of protein aggregation propensity: A self-interaction chromatography study. *Eur J Pharm Biopharm*. 2015;96:282–290.
11. Ahamed T, Ottens M, van Dedem GWK, van der Wielen LAM. Design of self-interaction chromatography as an analytical tool for predicting protein phase behavior. *J Chromatogr A*. 2005; 1089:111–124.
12. Xu X, Lenhoff AM. A predictive approach to correlating protein adsorption isotherms on ion-exchange media. *J Phys Chem B*. 2008;112:1028–1040.
13. Mollerup JM. Applied thermodynamics: A new frontier for biotechnology. *Fluid Phase Equil*. 2006;241:205–215.
14. Nfor BK, Ahamed T, van Dedem GWK, Verhaert PDEM, van der Wielen LAM, Eppink MHM, van de Sandt EJAX, Ottens M. Model-based rational methodology for protein purification process synthesis. *Chem Eng Sci*. 2013;89:185–195.
15. Nfor BK, Noverraz M, Chilamkurthi S, Verhaert PD, van der Wielen LA, Ottens M. High-throughput isotherm determination and thermodynamic modeling of protein adsorption on mixed mode adsorbents. *J Chromatogr A*. 2010;1217:6829–6850.
16. Mollerup JM, Hansen TB, Kidal S, Staby A. Quality by design–thermodynamic modelling of chromatographic separation of proteins. *J Chromatogr A*. 2008;1177:200–206.
17. Mollerup JM. The thermodynamic principles of ligand binding in chromatography and biology. *J Biotechnol*. 2007;132:187–195.
18. Hill TL. Thermodynamics for chemists and biologists. 1968.
19. Winzor DJ, Carrington LE, Harding SE. Analysis of thermodynamic non-ideality in terms of protein solvation. *Biophys Chem*. 2001;93:231–240.
20. Prausnitz JM, Lichtenthaler RN, de Azevedo EG. *Molecular Thermodynamics of Fluid-Phase Equilibria*. New Jersey: Pearson Education; 1998.
21. Hanke AT, Verhaert PD, van der Wielen LA, Eppink MH, van de Sandt EJ, Ottens M. Fourier transform assisted deconvolution of skewed peaks in complex multi-dimensional chromatograms. *J Chromatogr A*. 2015;1394:54–61.
22. Carta G, Jungbauer A. *Protein Chromatography: Process Development and Scale-Up*. Weinheim: Wiley-VCH Verlag GmbH & Co; 2010.
23. Zhang S, Iskra T, Daniels W, Salm J, Gallo C, Godavarti R, Carta G. Structural and performance characteristics of representative anion exchange resins used for weak partitioning chromatography. *Biotechnol Prog*. 2017;33:425–434.
24. Hagel L. Pore size distributions. In: Dubin PL, editor. *Aqueous Size-Exclusion Chromatography*. Amsterdam: Elsevier; 1988.
25. Zhu M, Carta G. Protein adsorption equilibrium and kinetics in multimodal cation exchange resins. *Adsorption*. 2016;22:165–179.
26. Staby A, Sand M-B, Hansen RG, Jacobsen JH, Andersen LA, Gerstenberg M, Bruus UK, Jensen IH. Comparison of chromatographic ion-exchange resins. III. Strong cation-exchange resins. *J Chromatogr A*. 2004;1034:85–97.
27. Wiendahl M, Schulze Wierling P, Nielsen J, Fomsgaard Christensen D, Krarup J, Staby A, Hubbuch J. High throughput screening for the design and optimization of chromatographic processes - Miniaturization, automation and parallelization of breakthrough and elution studies. *Chem Eng Technol*. 2008;31: 893–903.
28. Devices M. Making optical density measurements automatically corrected to a 1 cm pathlength in the SPECTRAmax® PLUS microplate spectrophotometer. https://www.moleculardevices.com/sites/default/files/en/assets/app-note/br/optical-density-measurements-automatically-corrected-to-1-cm-pathlength-with-path-check-technology.pdf. Accessed 09.05.2018.
29. Osberghaus A, Drechsel K, Hansen S, Hepbildikler SK, Nath S, Haindl M, von Lieres E, Hubbuch J. Model-integrated process development demonstrated on the optimization of a robotic cation exchange step. *Chem Eng Sci*. 2012;76:129–139.
30. Herrmann T, Schröder M, Hubbuch J. Generation of equally sized particle plaques using solid-liquid suspensions. *Biotechnol Prog*. 2006;22:914–918.
31. Huuk TC, Briskot T, Hahn T, Hubbuch J. A versatile noninvasive method for adsorber quantification in batch and column chromatography based on the ionic capacity. *Biotechnol Prog*. 2016;32:666–677.
32. Bergander T, Lacki KM. High-throughput process development: Chromatography media volume definition. *Eng Life Sci*. 2016; 16:185–189.
33. ThermoFisher Scientific. POROS™ Strong Cation Exchange Resins: XS and 50 HS. https://assets.thermofisher.com/TFS-Assets/LSG/manuals/100031321_POROS_StrongCationExchResins_PI.pdf. Accessed 01.11.2017.
34. Rakel N, Schleining K, Dismer F, Hubbuch J. Self-interaction chromatography in pre-packed columns: a critical evaluation of self-interaction chromatography methodology to determine the second virial coefficient. *J Chromatogr A*. 2013;1293:75–84.
35. Pirrung SM, van der Wielen LAM, van Beckhoven R, van de Sandt E, Eppink MHM, Ottens M. Optimization of biopharmaceutical downstream processes supported by mechanistic models and artificial neural networks. *Biotechnol Prog*. 2017;33:696–707.
36. Young M, Carroad P, Bell R. Estimation of diffusion coefficients of proteins. *Biotechnol Bioeng*. 1980;22:947–955.
37. Wilson EJ, Geankoplis CJ. Liquid mass transfer at very low reynolds numbers in packed beds. *Ind Eng Chem Fundam*. 1966;5:9. +.
38. Suzuki M, Smith JM. Axial dispersion in beds of small particles. *Chem Eng J*. 1972;3:256–264. (Supplement C):
39. Brenner H, Gaydos LJ. The constrained brownian movement of spherical particles in cylindrical pores of comparable radius: Models of the diffusive and convective transport of solute molecules in membranes and porous media. *J Colloid Interface Sci*. 1977;58:312–356.
40. Gunn DJ. Axial and radial dispersion in fixed beds. *Chem Eng Sci*. 1987;42:363–373.
41. LeVan MD, Carta G, Yon CM. Adsorption and Ion Exchange. In: Green DW, ed. *Perry's Chemical Engineers' Handbook*. New York: McGraw-Hill Companies Inc.; 1999:16–19.
42. Wu Y, Simons J, Hooson S, Abraham D, Carta G. Protein and virus-like particle adsorption on perfusion chromatography media. *J Chromatogr A*. 2013;1297:96–105.
43. Garke G, Hartmann R, Papamichael N, Deckwer WD, Anspach FB. The influence of protein size on adsorption kinetics and equilibria in ion-exchange chromatography. *Sep Sci Technol*. 1999;34:2521–2538.
44. Hofer S, Ronacher A, Horak J, Graalfs H, Lindner W. Static and dynamic binding capacities of human immunoglobulin G on polymethacrylate based mixed-modal, thiophilic and hydrophobic cation exchangers. *J Chromatogr A*. 2011;1218:8925–8936.
45. George A, Wilson WW. Predicting protein crystallization from a dilute solution property. *Acta Crystallogr Sect A Found Adv*. 1994;50:361.
46. Stellwagen E, Prantner JD, Stellwagen NC. Do zwitterions contribute to the ionic strength of a solution? *Anal Biochem*. 2008; 373:407–409.
47. Le Brun V, Friess W, Bassarab S, Muhlau S, Garidel P. A critical evaluation of self-interaction chromatography as a predictive tool for the assessment of protein-protein interactions in protein formulation development: a case study of a therapeutic monoclonal antibody. *Eur J Pharm Biopharm*. 2010;75:16–25.
48. Tessier PM, Lenhoff AM, Sandler SI. Rapid measurement of protein osmotic second virial coefficients by self-interaction chromatography. *Biophys J* 2002;82:1620–1631.
49. Susanto A, Knieps-Grünhagen E, von Lieres E, Hubbuch J. High throughput screening for the design and optimization of chromatographic processes: assessment of model parameter determination from high throughput compatible data. *Chem Eng Technol*. 2008;31:1846–1855.

Manuscript received Dec. 19, 2017, and revision received Apr. 12, 2018.